*Reprinted from:*

JOURNAL OF APPLIED PHYSICS VOLUME 42, NUMBER 5 APRIL 1971

# Analysis of a High-Explosive Shock-Tube Experiment*

H. David Glenn and Barbara K. Crowley
*Lawrence Radiation Laboratory, University of California, Livermore, California 94550*
(Received 19 August 1970)

A shock-tube experiment was performed with 5.5 kg of high explosives to generate and to drive an air shock down a steel pipe 7.8-cm i.d. and ~25-m length. Fiber optics and pressure transducers were installed at specific locations to record optical and pressure time of arrival of the air shock and pressure histories in the pipe. The initial~Mach 30 air shock attenuated to~Mach 6 at the end of the pipe. A numerical simulation of this experiment was performed. This paper presents the experimental arrangement and results, and briefly describes the numerical models used. The calculation results are compared with the data. During the interval of approximately 8 msec required for the shock to travel the length of the 25-m pipe, the calculations indicated that the predominant factors in attenuating the time of arrival of the shock were heat transfer and friction, respectively.

## I. INTRODUCTION

A variety of high-explosive (HE) shock tubes are used[1–5] to study high-energy shock propagation and its effects. Most shock tubes are designed in one of two categories discussed in the following paragraphs.

The first category includes those shock tubes designed to remain as permanent structures.[1,2] In these tubes, the driver section is usually designed with a small portion of its volume filled initially with HE. The effective driver pressure for shock propagation in these tubes is generally an order-of-magnitude below the detonation pressure, and shock velocities are considerably below detonation velocities.

The second category includes those tubes designed with the HE outside the driver section, and these are not permanent structures. When the HE burns, a driver plate moves[4,5] or the walls of the driver section collapse[3] to act as a piston on the gas existing in the driver section. Such designs can produce shock velocities two to five times the detonation velocities of the HE. However, a significant high-pressure region which could sustain these velocities does not generally exist behind these shocks.

A middle region [i.e., 0.1–1.0-cm/$\mu$sec shock velocities, 0.1–1.0-kb shock pressures, high-pressure (1–3 kb) retention (>100 $\mu$sec) in the driver section, etc.] exists between the above two categories.

A HE experiment was designed and conducted to study shock propagation in a long steel exit pipe (~25 m, 7.8 cm i.d.) containing the driven gas, atmospheric air. The present design has the advantages of (1) being able to impart enough energy to the driven gas of atmospheric air to generate shocks of 1.0 cm/$\mu$sec, (2) retaining high pressures in the HE driver section, (3) having a length-to-diameter ratio of >300, and (4) being a simple geometry which is readily adaptable to numerical simulation with existing time-dependent finite-difference codes. An accurate numerical simulation provides a calculational reproduction of the complete temporal and spatial history of the flow variables.[6]

This paper presents the data from the above experiment. The numerical models and calculations are presented, and the agreement between experimental data and calculations is shown. This paper demonstrates that experiments combined with numerical simulation can provide considerable information not obtainable by either purely experimental or analytical approaches.

## II. EXPERIMENTAL ARRANGEMENT

The shock-tube assembly and associated diagnostic instrumentation are depicted schematically in Fig. 1. A detonator and a plane-wave lens were used to initiate uniform burn in a 60-cm straight cylindrical section

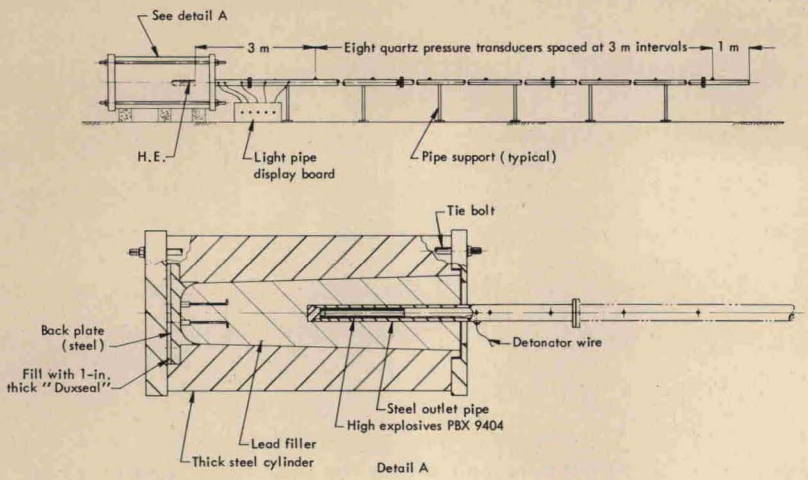


FIG. 1. HE shock-tube assembly and diagnostic coverage.

of HE (5.5-kg nitromethane PBX 9404 with a detonation velocity of ~8.8 mm/μsec). When the burn reached the end of the HE (~80 μsec), an air shock was initiated in the outlet pipe. The propagation of the air shock was monitored by optical and electronic diagnostics at regular intervals along the outlet pipe.

The detonated HE section ~7.8 cm diam and 60 cm long is the driver gas. High pressures in the driver section were retained by surrounding the HE with a high-density material (i.e., lead) and a thick steel cylinder.

The outer steel cylinder which enclosed the lead had a sufficiently high yield strength to restrain radial motion of the outer boundary of the lead cylinder. No direct radial path existed for the escape of HE gases. Motion of the lead in the axial direction was restrained by steel end plates secured by long 5-cm-o.d. steel rods (see Fig. 1). To detect and to record any physical motion or possible venting, front and rear portions of the HE housing were monitored by high-speed framing cameras.

Four light pipes[7] (fiber optics) were positioned at 60-cm intervals along the outlet pipe and a fifth (at 70 cm) was fitted with an aluminum reflector to view the front surface of the HE. The initiation and time of arrival (TOA) of the air shock for the first 2.4 m was determined with the above five light pipes. The light pipes were recessed in the steel wall about 3 mm and viewed the base through a 1-mm aperture in the wall. The light pipes were brought radially out of the outlet pipe and tied into a small display board. The luminosity associated with the shock front was transmitted via the light pipes to the display board which was scanned for approximately 500 μsec with a streaking camera. The light-pipe measurements provide an accurate means[5,8] of obtaining the shock arrival over the first several meters.

Eight standard Kistler quartz pressure gages were

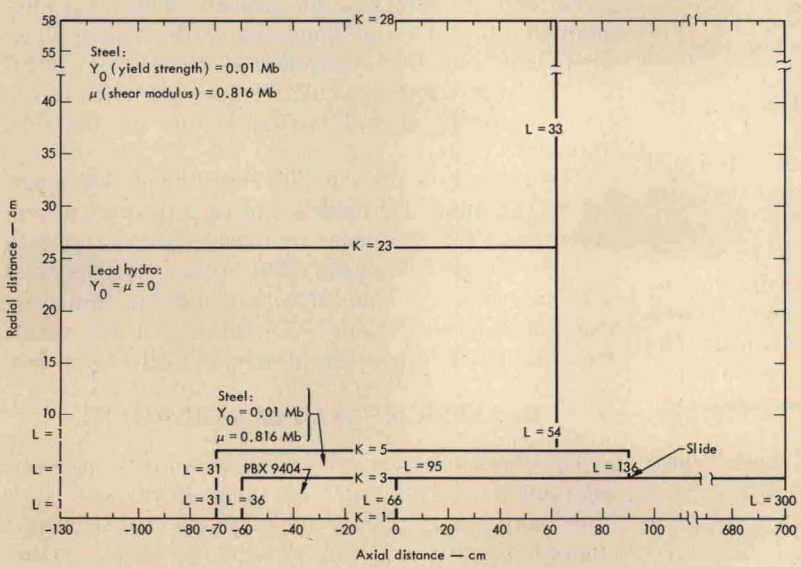


FIG. 2. Model used in HEMP numerical simultation of shock-tube assembly shown in Fig. 1. Horizontal ($L$) and vertical ($K$) zoning, yield strengths, and shear moduli assumed for different material regions are identified.

flush mounted at 3-m intervals along the outlet pipe. The signal from each transducer went through an emitter follower (~0.1-μsec rise time) to two scopes with appropriate sweep speeds and sensitivities that were determined from preshot estimates. The pressure transducers serve the dual purpose of providing TOA values and pressure-time histories for comparison with the calculations. Transducers 1, 3, and 5 were monitored with time-interval meters (TIM) to obtain microsecond accuracy on shock TOA with respect to the detonation signal.

## III. NUMERICAL CODES AND INITIAL CONDITIONS

The two numerical codes HEMP[9] and PUFL[10] used in the present study are described in the literature. Both codes use finite-difference calculational techniques to advance, with respect to time, the partial differential conservation equations of continuum mechanics. The following paragraphs briefly discuss the use of these codes in numerically simulating the present experiment.

### A. HEMP

HEMP is a two-dimensional Lagrangian code which is used here in cylindrical geometry. HEMP was used to simulate HE burn, the initiation of the air shock, and the radial wall motion in the HE region. The equations of state used in these calculations are given in Refs. 9 and 11.

### B. PUFL

PUFL is used here to simulate the one-dimensional axially symmetric flow in the pipe. PUFL considers friction and heat transfer which are not considered in HEMP.

### C. Numerical Calculation Model

Slight modifications of the actual experiment configuration (Fig. 1) were necessary in the numerical model illustrated in Fig. 2. These modifications are discussed below. Figure 2 also gives the yield strengths, dimensions, horizontal ($L$ lines) and vertical ($K$ lines) zoning, and other parameters pertinent to the calculations.

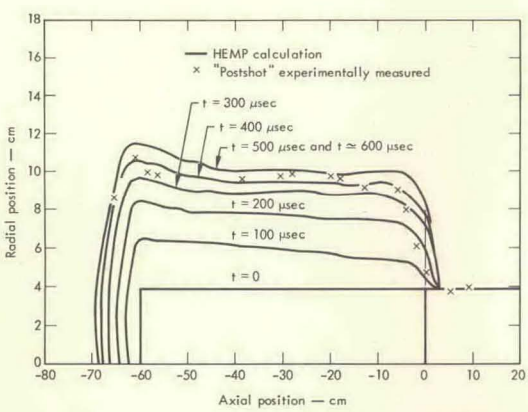


FIG. 3. Position of He–steel-wall boundary from HEMP plotted at 100-μsec intervals. "Postshot" measured values are also shown.

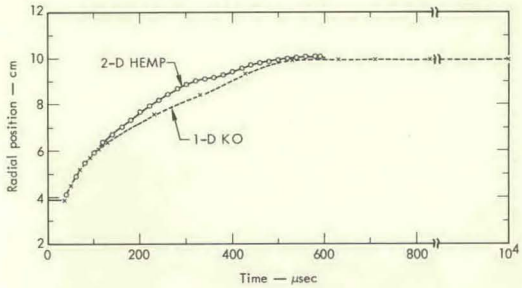


FIG. 4. Radial position of He–steel-wall boundary vs time (1-D KO code results and 2-D HEMP code results taken from axial midpoint of HE).

The calculations start with the initiation of detonation of the HE at the breech end of the 60-cm length of HE. No attempt was made to simulate the detonator or the plane-wave lens. Since the detonator and the plane-wave lens represent only a small portion (4.4 cm) of the total HE (64.4 cm), their omission is a minor perturbation. The end plates (Fig. 1) were also omitted in the numerical model. Other considerations in Fig. 2 are believed to be self-explanatory.

## IV. THEORETICAL AND EXPERIMENTAL RESULTS

### A. Source Region

For PBX 9404, with a detonation velocity of 0.88 cm/μsec, the HEMP code indicates peak pressures behind the detonation front of ~350kbar.[11] The wall motion in the HE section is illustrated in Fig. 3, which shows the radial position of the inner cylindrical steel pipe that surrounds the HE, at 100-μsec intervals. At approximately 500 μsec, the radial expansion reaches its maximum. The pipe then undergoes a small radial contraction due to the elastic properties of the outer steel cylinder. To obtain the radial pipe expansion of this region after 600 μsec, a one-dimensional KO code[9] calculation in cylindrical geometry was considered. The results of this calculation are given in Fig. 4 along with the first 600-μsec results from HEMP for comparison. Figure 4 shows the HEMP results plotted for the midpoint position of the HE where the end effects are reduced. Figure 4 implies that the radial motion essentially ceases after 600 μsec.

Axial and radial measurements of this HE region were taken postshot and are given in Fig. 3 for compariosn with the calculated values. Radial variations at a given axial position were generally small ($\leq$0.2 cm). Postshot observation also indicated that the inner steel cylinder remained intact with no fragmentation.

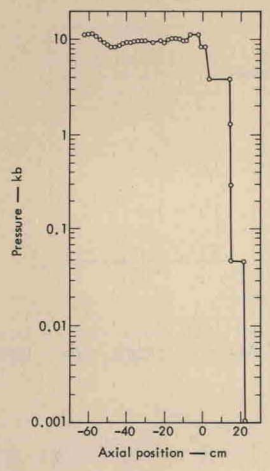


(a)

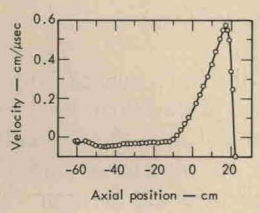


(b)

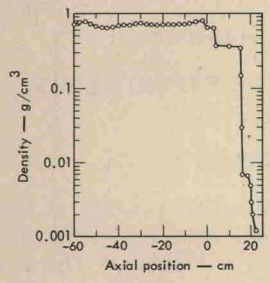


(c)

FIG. 5. HEMP code results at 100 μsec for (a) pressure, (b) velocity, and (c) density.

Cracks in the axial direction occurred near the HE–air interface, which is consistent with late time (>1.0 msec) venting which was experimentally observed and is discussed below. Postshot measurements of the outer steel cylinder indicated that no permanent deformation occurred.

Framing camera coverage (90-μsec interframe time) of the front section of the HE housing gave photographic evidence that HE gases vented from the source region. Venting to the atmosphere was first observed at 1.04 msec and continued until approximately 4.4 msec, after the HE was detonated. No gross motion of the outlet pipe or lead was noted for the 10-msec duration of the framing camera coverage. Postshot examination of the source region and framing film indicated that the venting path was radial through cracks in the inner steel pipe and lead housing. The venting path was then axial through the shock-induced separation between the lead housing and outer steel cylinder. Consequently, the loss of HE gases from the driver section began much earlier than the 1.04 msec observed by photographic coverage of the front surface of the HE housing. This loss of driver gas was considered in the calculations presented later. It is shown that the loss of driver gas had a negligible effect on the TOA results, but it did affect the pressures well behind the shock front. Framing camera coverage of the rear section of the HE housing indicated that no venting occurred from this region for the duration (~10 msec) of the experiment.

At 100 μsec, detonation of the HE is completed, and the air shock is starting to form. The velocity, density, and pressure from HEMP at 100 μsec are shown in Figs. 5(a)–(c). These HEMP conditions are used as initial conditions for PUFL. Also, the pipe radius as a function of time and axial position from HEMP (Fig. 3) was used for the pipe-radius boundary condition in PUFL. Because of the KO results in Fig. 4, at times greater than 600 μsec, the radii are assumed to remain constant.

The feasibility of using the quasi-one-dimensional PUFL code to simulate the pipe flow is illustrated in Fig. 6. This figure shows the pressure vs axial position as calculated by both HEMP and PUFL at 500 μsec. Comparisons at earlier times give even closer agreement.

### B. TOA Results

To correlate the optical and electronics measurements, a common time reference was provided by the electrical signal which initiated detonation of the plane-wave lens. The elapse time between the detonation signal and luminosity record for initiation of the air shock was experimentally measured as 80.6 μsec. This luminosity record was obtained with the streaking camera and the aluminum-reflector-adapted light pipe mentioned previously. The elapse time compares with a 77.1-μsec calculated elapse time which is obtained by

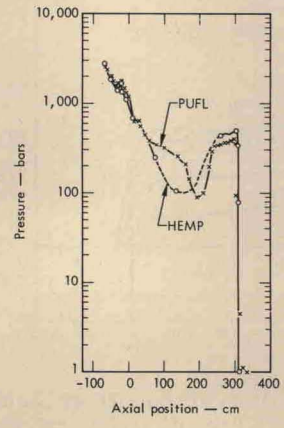


FIG. 6. Pressure vs axial position from both HEMP and PUFL codes at 500 μsec.

summing up the detonator, the plane-wave lens, and the HE-cylinder burn times. The difference can be partially attributed to the time necessary to shock the air adjacent to the HE. In order to simplify, in the following experimental and theoretical results presented here, the 80.6-$\mu$sec air shock initiation time will be taken as the new zero time reference for TOA data.

Figure 7 shows the experimental TOA data obtained from the light pipes and pressure transducers. The shock velocity, obtained by taking slopes of the TOA curve in Fig. 7, decreased from 1 cm/$\mu$sec near the HE to 0.2 cm/$\mu$sec at the end of the pipe. The time-interval meters indicated shock TOA of 0.467, 1.819, and 3.675 msec for the pressure transducers at 3, 9, and 15 m, respectively. These results are in good agreement with the scope records for these transducers.

A complete simulation of the venting associated with the HE region is not feasible. One limiting situation is no venting. The PUFL calculation which simulated no venting retained all of the HE gas and air from the HEMP calculations (shown in Fig. 5) within the boundaries shown in Fig. 4. The TOA results from this PUFL calculation, labeled P-1, included the effects of friction and heat transfer, and are shown (in Fig. 7) to agree favorably with the experimental TOA data.

One approximation for venting is that all of the HE with a negative velocity at 100 $\mu$sec after detonation

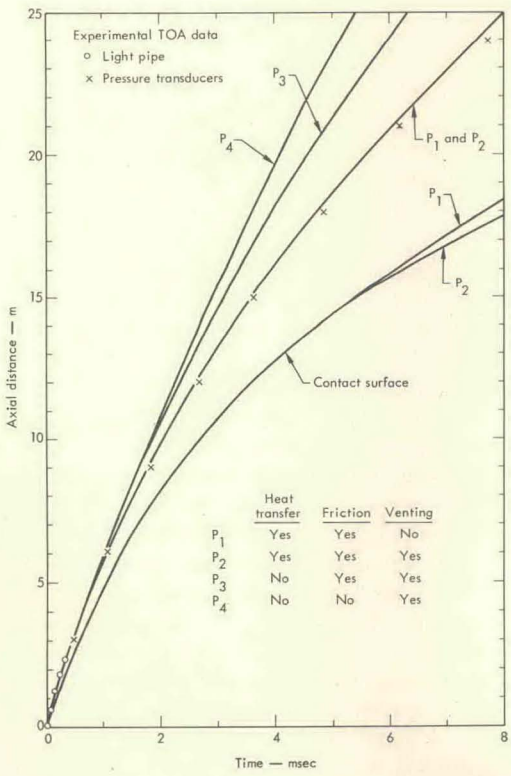


FIG. 7. Experimental and calculated shock position vs time.

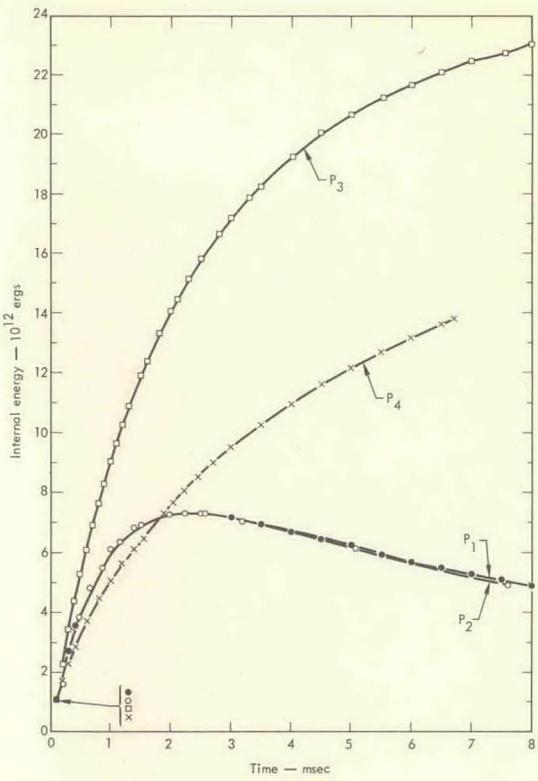


(a)

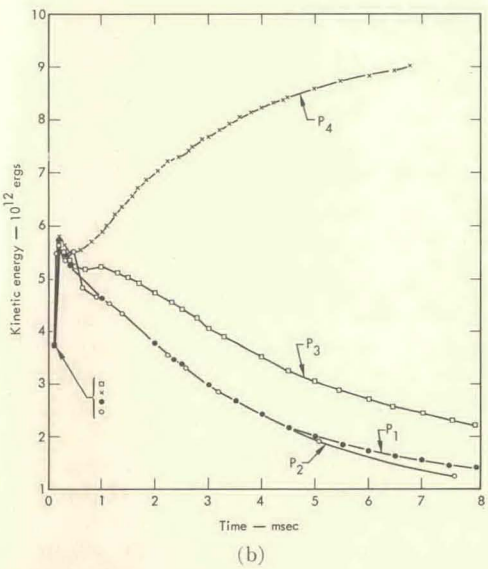


(b)

FIG. 8. Results for driven air gas from PUFL; (a) internal energy versus time and (b) kinetic energy vs time.

vents—see Fig. 5(b). The PUFL calculations for venting omit all material with negative velocities in Fig. 5(b). Further, it can be conservatively approximated that starting at 100 $\mu$sec after detonation, the left boundary of the material with positive velocities is exposed to atmospheric pressure. This approximation

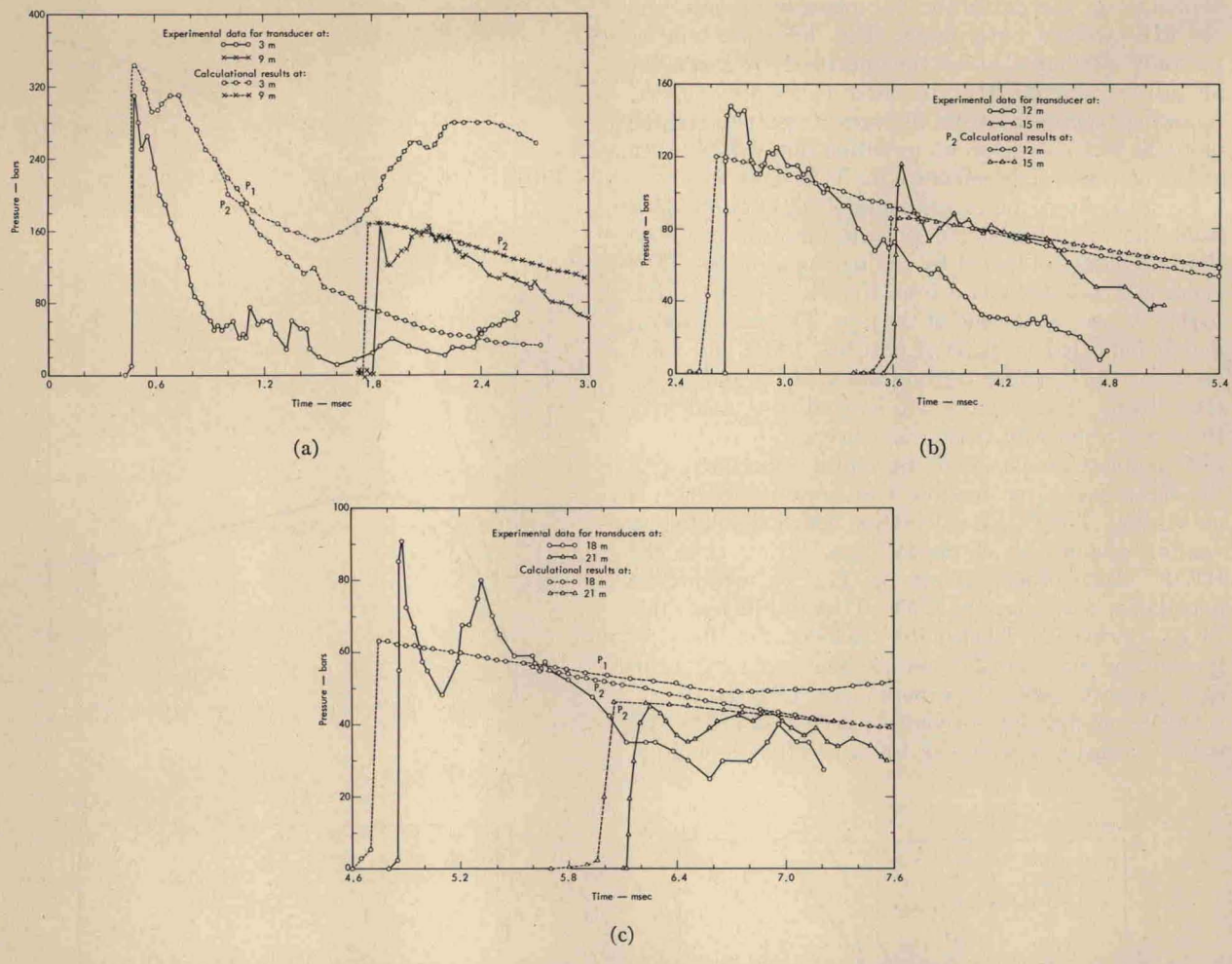


FIG. 9. Pressure vs time from pressure transducers and calculations at (a) 3 and 9 m, (b) 12 and 15 m, and (c) 18 and 21 m. Square denotes calculated arrival of contact surface.

is incorporated into the PUFL calculation by assigning one bar of pressure to the left boundary. The PUFL calculation *P*-2, for which these boundary approximations were used and in which and the effects of friction and heat transfer were considered, also gave very reasonable agreement with the TOA data (see Fig. 7).

The agreement in TOA results from these two PUFL calculations, in which venting and no venting were considered, indicates that the venting did not detectably affect the TOA data. Calculational results for the contact surface TOA's are given in Fig. 7 for the P-1 and P-2 cases. Rarefaction (from venting) does not appear to affect the motion of the contact surface for times less than 5 msec.

The P-1 and P-2 PUFL calculations considered the effects of convective heat transfer and friction. Preshot measurements in the exit pipe indicated an average "pipe radius-to-surface roughness" ratio of greater than 1000. Hence, the pipe was considered smooth, and a dimensionless friction coefficient of $C_f/2=0.002$ was chosen[12] for the calculations. It is assumed that the Reynolds' analogy holds and that the Stanton number is also 0.002.

To investigate the relative effect of heat transfer and friction, two additional PUFL calculations, P-3 and P-4, were considered. In these calculations the same venting approximation as P-2 was used, and their TOA results are also shown in Fig. 7. In the P-4 calculation both heat transfer and friction were omitted. In the P-3 calculation heat transfer was omitted, but the effect of friction was considered. Figure 7 indicates that heat transfer significantly affects the TOA results.

In Figs. 8(a) and(b) the internal and kinetic energies in the air region are shown, respectively, as a function of time from the four calculations. In Fig. 8(a), the P-1 and P-2 calculations give nearly identical results out to 7 msec. This is further evidence that venting did not affect the time history of the shocked-air region.

There is no heat transfer in either the P-3 or P-4 calculations, and their internal and kinetic energies in Fig. 8 are both higher than those of the P-2 calculation with heat transfer. In the P-3 calculation friction converts kinetic energy into internal. The P-4 calculation which uses no friction is seen in Fig. 8 to have larger kinetic energy and smaller internal energy than the P-3 with friction. The P-4 calculation also has a higher shock velocity (Fig. 7) than does P-3.

### C. Pressure Histories

Pressure histories were experimentally obtained from quartz gages located at 3, 9, 12, 15, 18, and 21 m from the front surface of the HE cylinder. The gages located at 6 and 24 m provided only TOA results. The pressure-response results have been corrected for the amplification ($\sim$0.95) due to the emitter followers. Insulation from thermal effects was provided with a 0.5-mm ablative coating on the surface of the gage. The KO code[9] calculations indicate a time of only 0.3–0.4 $\mu$sec for a pressure pulse to transit the ablative coating, the thin steel diaphragm, and the quartz crystal before conversion to an electrical signal. This slight inherent delay has been ignored in the data presented.

Figures 9(a)–9(c) present the corrected experimental pressure results and the corresponding P-2 calculational results for the above six transducers. The calculational results are based on the venting criteria discussed earlier. The principal effect of the observed venting was to reduce pressures well behind the shock front. This fact is illustrated in Figs. 9(a) and 9(c), which also show the pressure histories at 3 and 18 m for the P-1 (no venting) calculations. These figures also indicate that venting appears to have little influence on the peak pressures in the shock front.

## V. DISCUSSION AND CONCLUSIONS

The calculations indicate that in the energy range of this experiment, heat transfer and friction are the predominant factors in attenuating the shock velocity from 1 to 0.2 cm/$\mu$sec (over approximately 25 m of propagation). Further, an attempt has been made to identify the rarefaction effects (of the observed venting) on the shock-front and contact-surface TOA, the pressure histories, and the kinetic and internal energies of the shocked air. The principal rarefaction effect for this experiment appears to be limited to the reduction of pressures well behind the shock front.

It is shown that the HE air-shock experiment is capable of accurate numerical simulation with existing finite-difference calculations. It is demonstrated that these calculations provide considerable information not accessible by analytical or purely experimental means.

## ACKNOWLEDGMENTS

The authors would like to express their appreciation to B. L. Maranville and D. G. Garner for engineering designs, to P. L. Turner for electronics support, to T. L. Schaffer for mechanical assembly support, to A. R. Licuanan for the HEMP calculations, and to E. A. Reed for the PUFL calculations.

* Work performed under the auspices of the U.S. Atomic Energy Commission.

[1] B. P. Bertrand, in Conf. Military Applications Blast Simulators, Suffield, Canada, 1967.

[2] D. W. Culbertson, in Proc. Seventh International Shock Tube Symposium, Toronto, Canada, 1969.

[3] S. P. Gill, Stanford Research Institute Report No. TR0001-66, 1966.

[4] A. E. Voitenko, Sov. Phys. Tech. Phys. **11**, 128 (1966).

[5] H. D. Glenn and B. K. Crowley, Lawrence Radiation Laboratory, Livermore, Report No. UCRL-71007, 1968.

[6] B. K. Crowley and H. D. Glenn, in Proc. Seventh International Shock Tube Symposium, Toronto, Canada, 1969.

[7] N. S. Kapany, *Fiber Optics* (Academic, New York, 1967).

[8] H. D. Glenn and B. K. Crowley, J. Appl. Phys. **41**, 689 (1970).

[9] M. L. Wilkins, in *Methods in Computational Physics* edited by B. Alder, S. Fernbach, and M. Rotenberg (Academic, New York, 1964), Vol. 3.

[10] B. K. Crowley, J. Comp. Phys. **2**, 61 (1967).

[11] M. L. Wilkins, Lawrence Radiation Laboratory, Livermore, Report No. UCRL-14531, 1965.

[12] H. Schlichting, *Boundary Layer Theory* 2nd ed. (McGraw-Hill, New York, 1960).